Plasmonics (2023) 18:407–420
https://doi.org/10.1007/s11468-022-01771-z

Multipole Plasmonic Optical Properties of the Au Cone-On-Plate Nanostructure: Change the Effective Mean Free Path to Improve Refractive Index Sensing

Yu-Bo Guo[1] · Jian Zhu[1] · Guo-Jun Weng[1] · Jian-Jun Li[1] · Jun-Wu Zhao[1]

Received: 3 November 2022 / Accepted: 12 December 2022 / Published online: 30 December 2022

Abstract
In this study, a novel structure, the Au cone-on-plate nanostructure, has been proposed, which can substantially improve the refractive index (RI) sensitivity of the Au nanocone. The plasmonic properties of the Au cone-on-plate nanostructure have been investigated by the discrete dipole approximation (DDA). The presence of the Au nanoplate can effectively reduce the full width at half maximum (FWHM) of local surface plasmon resonance (LSPR) from the Au nanocone. The analysis of the local electric fields indicates that the Au nanoplate can influence the FWHM of multipole resonance (l = 3) peak by changing the effective mean free path of polarized charges. We use three parameters to evaluate the RI sensitivity: the figure of merit (FOM), the bulk sensitivity (ηB), and the $\eta B \times$FOM. By adjusting the thickness of Au nanoplate (T) and the space between Au nanoplate and Au nanocone (S), the RI sensitivity could be well tuned. When $T = 5$ nm and $S = 2$ nm, the FWHM can be reduced from 220 to 80 nm, $\eta B = 500$ nm/RIU, FOM = 6.25 RIU^{-1}, and $\eta B \times$FOM = 3125 nm/RIU^2, which is seven times that of the Au nanocone. It shows excellent potential in the RI sensitivity of Au nanoparticles. The above results suggest the Au nanoplate can influence the distribution of polarized charges thereby substantially improving the RI sensitivity. This expands more possibilities for the Au nanocone in plasmonic sensing.

Keywords Local surface plasmon resonance (LSPR) · Au cone-on-plate nanostructure · Effective mean free path · Multipole plasmon resonance · Refractive index sensitivity

Introduction

Noble metal nanoparticles have unique optical properties due to their local surface plasmon resonance (LSPR) properties, which make them promising for a wide range of applications in solid-state electronics [1, 2], surface science [3], nanophotonics [4, 5], chemistry [6, 7], biosensing [8–10], enhanced spectroscopy [11–14], and so on. The collective oscillation behavior of electrons on the metal surface under the influence of light, due to the different shape, size, and material of nanostructures, causes the change of extinction (absorption and scattering) cross section related to wavelength [15]. Au [16], Ag [17], Pd [18], and Pt [19] are the most common noble metal nanostructures in plasmonic sensing based on LSPR. In addition, plasmonic sensing of composite metals [20], two-dimensional nanofilms [21], and three-dimensional nanoarrays [22] have also been investigated. Among them, Au and Ag are considered as important materials in plasmonic sensing due to their chemical stability, and excellent spectral properties. Therefore, Au and Ag plasmonic sensors are considered as an efficient and sensitive diagnostic method. In recent years, plasmonic sensors have been widely used in many applications. Reyes-Coronado et al. found that the coherent scattering model (CSM), 2D dipole model (2D-DM) and Maxwell Garnett model (MGM) methods are applicable to plasmonic sensing simulations for different cases. And all three are applicable when the coverage and particles are small. And the reflectivity changes when the nanoparticles are arranged in different

✉ Jian Zhu
nanoptzj@163.com

✉ Jun-Wu Zhao
nanoptzhao@163.com

[1] The Key Laboratory of Biomedical Information Engineering of Ministry of Education, School of Life Science and Technology, Xi'an Jiaotong University, Xi'an 710049, China

ways as a thin film on the base substrate [23]. Based on the effective medium theory, Solis-Tinoco et al. theoretically and experimentally verified the possibility of the thin gold nanofilm as biosensors depending on the change of refractive index [24]. Usually, plasmonic sensor performance is compared by the performance of RI sensitivity. In sensing based on the LSPR peak shift of noble metal nanoparticles, RI bulk sensitivity is defined as the offset of the LSPR wavelength divided by the change in refractive index in RIU/nm ($\eta B = \Delta\lambda peak/\Delta n$) [25]. High sensitivity means that a small change in refractive index causes a dramatic change in the LSPR wavelength, which is of great advantage in molecular detection. The quality factor is defined as the refractive index sensitivity divided by FWHM in RIU^{-1} (FOM = ηB/FWHM) [26]. Low FWHM and high ηB will cause a large FOM. $\eta B \times$ FOM is used to evaluate the overall performance of the sensor [26].

Much of the literature is devoted to the study of noble metal nanoparticles in RI sensitivity. For example, Tam et al. found that the silica-Au nanoshell structure has a high sensitivity in spherical nanoparticles with $\eta B = 554$ RIU/nm, but its FWHM is as high as 498.6 nm, leading to FOM = 0.9 RIU^{-1} [27]. This poor sensitivity makes it almost worthless in practical application. Based on this conclusion, Takei et al. proposed a half-capped silica-Au nanoshell, which ensures a high refractive index sensitivity and can make FOM = 2.5 RIU^{-1} by reducing the FWHM to about 200 nm [28]. In summary, an obvious problem of noble metal nanoparticles is that ensuring high ηB while causing large FWHM, which results in low FOM. Therefore, reducing the FWHM has become the focus of the RI sensitivity.

FWHM can be defined as the corresponding bandwidth value at half of the LSPR peak in the spectrum [29]. The peak width of LSPR is mainly due to the electron oscillations on the surface, which is related to damping. And this damping is caused by the scattering of electrons by collisions with other substances, such as phonons, electrons, impurities, and so on [30]. For metal nanoparticles, the scattering of conduction electrons from the surface leads to the variation of the effective mean free path and damping, which is the main reason for the variation of the peak bandwidth [31]. The material, morphology, and size of the noble metal nanoparticles can affect the electron scattering process and FWHM consequently [15]. Zhu et al. investigated the effect of nonuniform silver coating on the bandwidth of equipartition excitations in Au–Ag core–shell nanorods. The result shows that FWHM decreases with the increase of silver coating thickness. This is mainly because silver has a larger scattering relaxation time than gold [32]. Thus, the silver coating can reduce the FWHM of Au nanorods. Dimer nanostructures exhibit excellent properties beyond monomers in many ways [33]. Sajid Farooq et al. conducted a systematic study of refractive index sensing of tip-to-tip Au nanorod dimer by finite element analysis and found that when the aspect ratio is 8, $\eta B = 527$ nm/RIU and FOM = 10.532. Most importantly, the FWHM can be reduced to half of the monomer [26]. However, stable dimers are more difficult to achieve in the process. Li et al. found that the Au nanobipyramid has lower FWHM while maintaining higher RI sensitivity because of the tips form a strong hot spot region [34]. Weng et al. found that the resonance mode of Au nanobipyramid belongs to multipole resonance [35]. Therefore, slender nanostructures with tips have multipole resonance modes and show higher sensing potential. However, the regulation of FWHM is almost aimed at dipole resonance. How to effectively regulate the multipole resonance to get smaller FWHM and higher RI sensitivity is important.

Au nanocone is one of the slender nanostructures with a nanoscale tip. With the development and popularity of nanoimprint lithography, Au nanocone has become a hot spot in multifaceted research. For example, Choa et al. systematically investigated the photothermal efficiency of gold nanocones. Due to the hot spots, the extra-long nanocone can generate a major heat source at the apex, thus offering the possibility of reducing the spatial size of the heat source from the whole nanostructure to some of its parts [36]. Zhu et al. designed a biomarker chip using the strong hot spot of the Au nanocone [37]. In addition, the Au nanocone prepared by experiments has been widely used in plasmonic catalyst [38], enhancement spectroscopy [39], and gas detection [40]. How to improve its sensing capability becomes the focus of its application. Herein, we propose a new structure: Au cone-on-plate nanostructure. The refractive index (RI) sensitivity of the Au con-on-plate nanostructure is studied by discrete dipole approximation (DDA). By changing the thickness of Au nanoplate (T) and the space between Au nanoplate and Au nanocone (S), FWHM and FOM are discussed. And the physical mechanism is explained by mapping the local electric fields.

Models and Calculation Methods

DDA Simulation

In the theoretical calculation of the LSPR of noble metal nanoparticles, the following methods are commonly used: Finite difference in the time domain (FDTD) [41], finite element method (FEM) [42], and discrete dipole approximation (DDA) [43]. The DDA method decomposes nanoparticles into independent dipoles and calculates the interaction of each dipole with the electromagnetic field [44].

To summarize, DDA uses a finite number of dipoles (N) to simulate the shape of the target. Then, the optical

Table 1 RI sensitivity of the Au nanocone

	n = 1.33	n = 1.34	n = 1.35	n = 1.36	n = 1.37	n = 1.38	n = 1.39
FWHM (nm)	222						
λpeak (nm)	692	695	698	701	704	707	710
ηB (nm/RIU)	300						
FOM (RIU^{-1})	1.5						
ηB×FOM (nm/RIU^2)	450						

Table 2 RI sensitivity of the Au cone-on-plate nanostructure with $T = 11$ nm and $S = 2$ nm

	n = 1.33	*n* = 1.34	*n* = 1.35	*n* = 1.36	*n* = 1.37	*n* = 1.38	*n* = 1.39
FWHM (nm)	70						
λpeak (nm)	700	704.3	708.6	713	717.3	721.6	726
ηB (nm/RIU)	433						
FOM (RIU^{-1})	6.19						
ηB×FOM (nm/RIU^2)	2680.27						

response of the geometric parameters to the target shape is calculated under the given conditions [45]. Based on the DDA approach, Flatau and Draine developed a free and open Fortran-90 package: the code for DDSCAT 7.3 [46, 47]. The number of polarizable dipoles (*N*) of the target has a great influence on the calculation results of the optical properties [44]. Therefore, in order to ensure the convergence of the model represented by the polarizable dipole (*N*), the distance between the polarizable dipoles must be less than 1 nm. In other words, the number of dipoles *N* must be greater than 10^4 [48].

Geometrical Shape and Parameters of Au Cone-On-Plate Nanostructure

As shown in Fig. 1, the Au cone-on-plate nanostructure consisted of two parts. The lower part is the Au nanoplate which has two main geometric parameters: the side length L = 200 nm and the thickness (*T*) changing from 5 to 14 nm. The upper part is the Au nanocone with the diameter D = 100 nm and the height of the bottom surface H = 100 nm. The space between the Au nanocone and the Au nanoplate (*S*) changes from 2 to 11 nm. The origin of the coordinates (o) is at the center of the bottom surface of the lower Au nanoplate. The incident light *k* is parallel to the *x* direction and the polarization direction *E* is parallel to the *z* direction. The dipole distance is set to 1 nm. The Au nanocone consists of 17,173 dipoles and the Au nanoplate consists of at least 200,000 dipoles. Both are greater than 10^4. This ensures the accuracy of the simulation results. The refractive index of the medium is 1.33, which is the refractive index of water [35]. In addition, the frequency-dependent dielectric function of Au nanoparticles applied in the calculations was referred to in the report of Johnson and Christy [49].

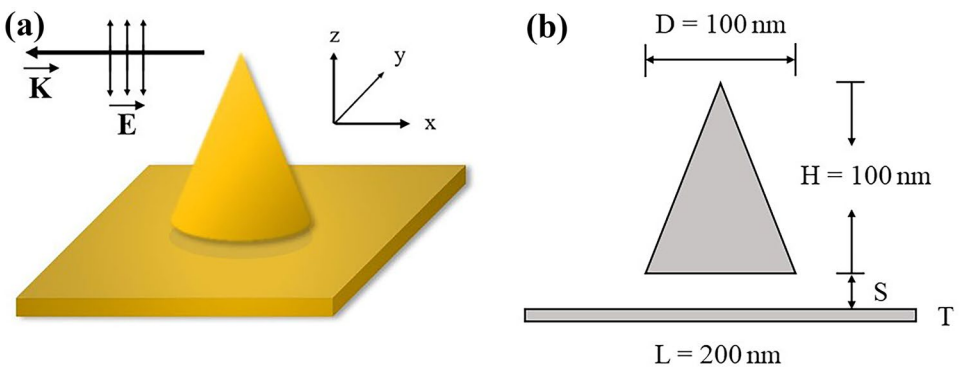

Fig. 1 **a** The 3D view of the Au cone-on-plate nanostructure. *k* means the direction of light and *E* represents the direction of polarization (TM). **b** The *xoz* plane of Au cone-on-plate nanostructure

Table 3 The comparison of the RI sensitivity parameters between the Au cone-on-plate nanostructure and other previously reported Au plasmonic structures of other morphologies

Morphology	$\eta B \times$FOM (nm/RIU^2)	ηB (nm/RIU)	FWHM (nm)	FOM (RIU^{-1})	Reference
Au nanoshell	2057.4	381	71	5.4	[57]
Au nanobipyramid	1584.0	352	78	4.5	[34]
Au dimer nanoplates	1400	350	88	4.0	[33]
Au nanodisc	750.0	300	120	2.5	[58]
Au nanorod	269.3	201	150	1.34	[59]
Au cone-on-plate nanostructure	3125.0	500	80	6.25	This work

Results and Discussion

Plasmonic Optical Properties of the Au Nanocone and the Au Cone-On-Plate Nanostructure

The extinction spectrum of the Au nanocone with D = 100 nm, H = 100 nm, and n = 1.33–1.39 is calculated by DDSCAT software, as shown in Fig. 2a. n = 1.33–1.39 is the variation of the refractive index of the medium around the Au nanocone. The variation of $\lambda peak$ with n = 1.33–1.39 is shown in Fig. 2b. $\lambda peak$ increases linearly with increasing n. The Au nanocone only has one distinct extinction peak at 690 nm with n = 1.33. This is consistent with the gold nanocone extinction cross section with AR = 1 simulated in

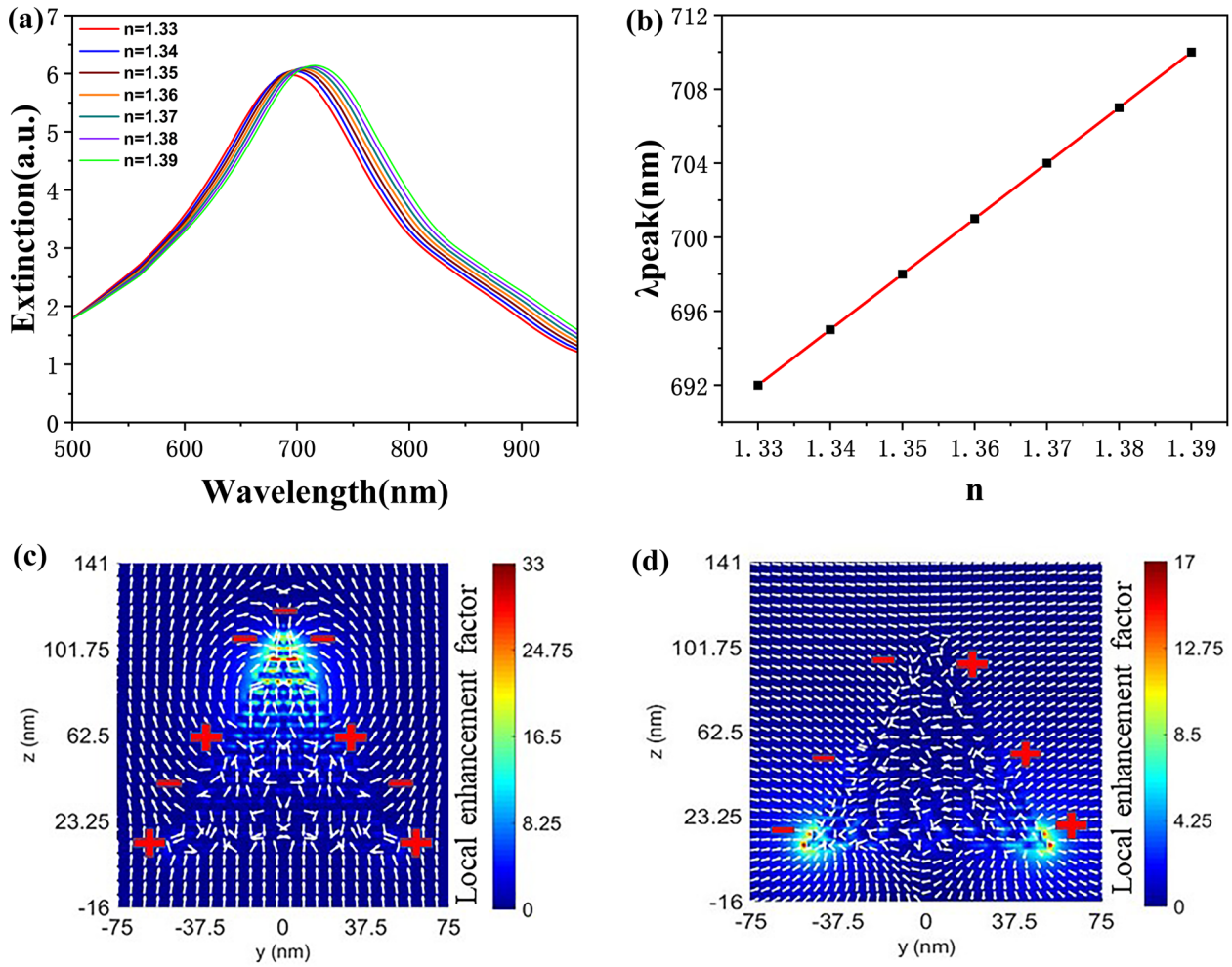

Fig. 2 **a** The extinction spectrum of the Au nanocone with n = 1.33–1.39. **b** $\lambda peak$ with the change of n between 1.33 and 1.39. $\lambda peak$ means the resonance wavelength of the extinction peak. **c** The local electric field in the *yoz* plane of the Au nanocone at 692 nm with n = 1.33 (TM). **d** The local electric field in the *yoz* plane of the Au nanocone at 542 nm with n = 1.33 (TE)

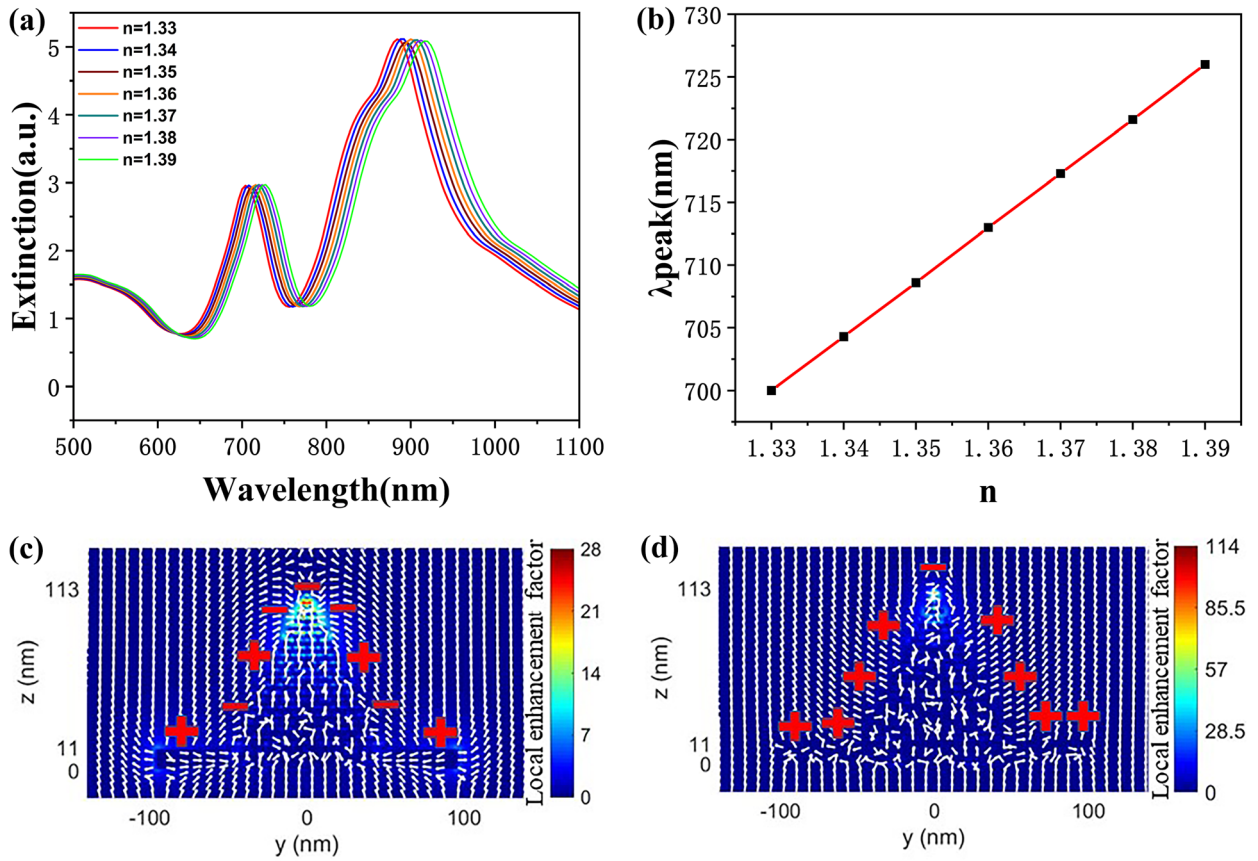

Fig. 3 **a** The extinction spectrum of the Au cone-on-plate nanostructure with $n = 1.33$–1.39. **b** $\lambda peak$ with the change of n between 1.33 and 1.39. **c** The local electric field in the *yoz* plane of the Au cone-on-plate nanostructure at 700 nm with $n = 1.33$ (TM). **d** The local electric field in the *yoz* plane of the Au cone-on-plate nanostructure at 900 nm with $n = 1.33$ (TM)

FEM by Cunha et al. [36]. However, they did not identify the source of this extinction peak. In order to determine the cause of this extinction peak, we simulate the local electric field at 692 nm along the *yoz* cross section with $n = 1.33$ (TM) in Fig. 2c. It is obvious that a large amount of negative polarized charges is concentrated at the tip and the positive polarized charges are mainly distributed at the sides. But a small number of opposite charges is distributed at the sides of the Au nanocone near the two endpoints. Through the explanation of the specific mechanism in "Multipole plasmon resonance in the Au nanocone" section, it can be determined that this distinct extinction peak belongs to the multipole resonance (l = 3). However, as shown in Fig. 2d, the local electric field along the *yoz* cross section of the Au nanocone (TE) shows that the polarized charges are distributed at the bottom edge. In TE polarization, the tip of the nanocone is not utilized, and the current studies on tip nanoparticles are focused on the utilization of the tip. Besides, the multipole resonance (l = 3) of the Au nanocone is only presented in the TM polarization. Therefore, in this paper, we all use the TM polarization.

As the refractive index of the surrounding medium increases, the extinction peak is red-shifted due to the decrease in the repulsive force between dipoles in the same direction, resulting in a decrease in the energy of proton oscillations [50]. The RI sensitivity of the Au nanocone is shown in Table 1. As n increases from 1.33 to 1.39, the FWHM is stabilized up to 222 nm and the $\lambda peak$ increases uniformly from 692 to 710 nm. Therefore, it can be calculated that $\eta B = 300$ nm/RIU, $\mathrm{FOM} = 1.5\ \mathrm{RIU}^{-1}$ and $\eta B \times \mathrm{FOM} = 450\ \mathrm{nm/RIU}^2$. According to the results, the Au nanocone is relatively low in RI sensitivity. One of the main factors is the large FWHM.

Due to the high FWHM of the Au nanocone, its performance in RI sensitivity is very poor. Reducing FWHM becomes the most effective way to improve the sensitivity. Morales-Luna et al. studied the doping of plasmonic nanoparticles (Au, Ag, Au) with other media (different phases of molybdenum trioxide (MoO3)) which results in a dramatic change in optical property. The small FWHM is related to different phases of MoO3 thin films doped with different nanoparticles at different volume filling fractions

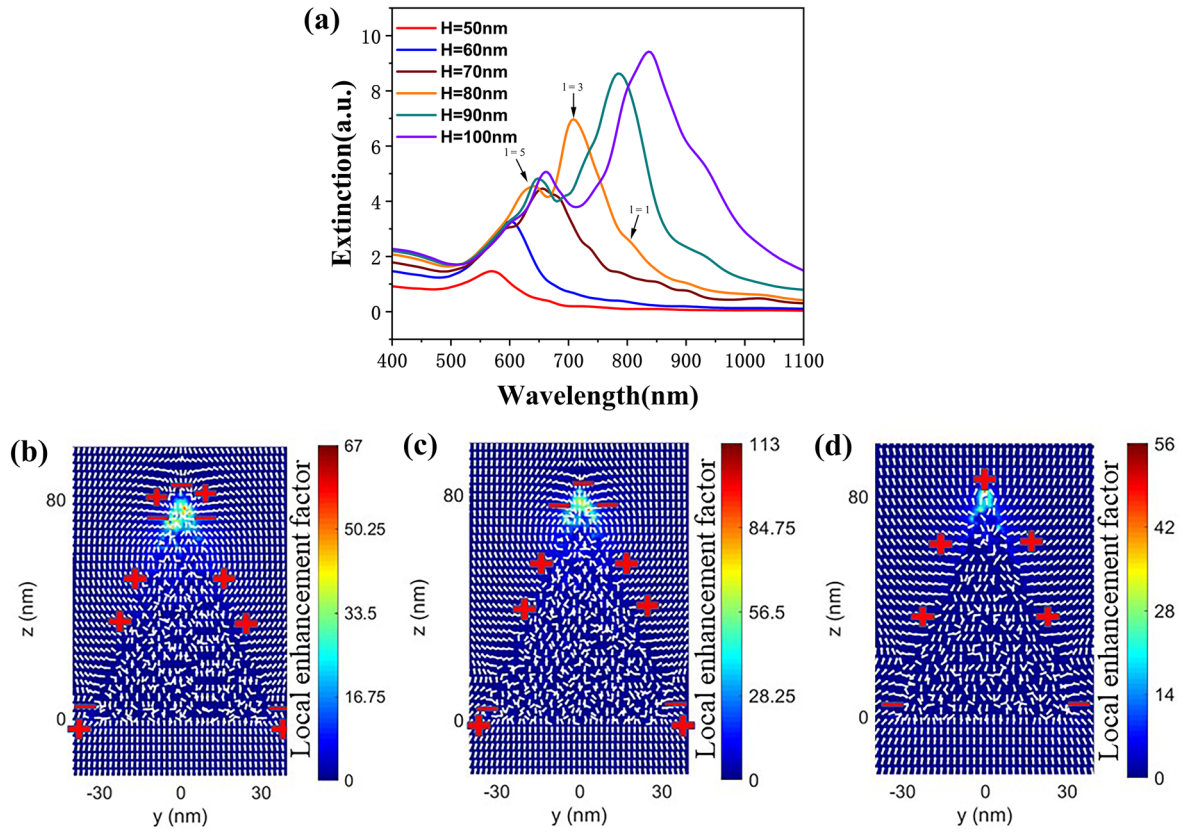

Fig. 4 **a** The extinction spectrum of the Au nanocone with D = 60 nm, H = 50–100 nm, n = 1.33. The local electric field in the *yoz* plane of the Au nanocone at **b** 620 nm, **c** 750 nm, and **d** any weak peak after 800 nm

[51]. When the nanostructure is fabricated on a metallic substrate, the scattering process of conduction electrons on the particle surface can be greatly altered and affect the FWHM [52]. According to this phenomenon, we propose the Au cone-on-plate nanostructure. Figure 3a shows the extinction spectrum of the Au cone-on-plate nanostructure with T = 11 nm, S = 2 nm, and n = 1.33–1.39. The Au cone-on-plate nanostructure has two obvious extinction peaks at 700 nm and 900 nm with n = 1.33. The local electric fields in these two resonance wavelengths, along the *yoz* cross section through the center and apex of the bottom surface, are shown in Fig. 3c, d. In noble metal nanoparticles, the scattering of light affects the polarized charges distribution. Thus, the scattering can be illustrated by analyzing the polarized charges distribution. The polarized charges distribution of the Au nanocone is "−" "+" "−" "+" in Fig. 2c. However, as shown in Fig. 3c, the polarization charges distribution of the Au nanocone part is "−" "+" "−". According to the LSPR of noble metal nanoparticles, the polarized charges are all in pairs. Through the distribution of the local electric field, it can be found that the negative polarized charges at the bottom of the nanocone are coupled with the positive polarized charges on the upper surface of the nanoplate. Therefore, the resonance of the whole system is the multipole resonance (l = 3) of the Au cone-on-plate nanostructure. Besides, the polarized charges distribution of the extinction peak at 900 nm changes significantly. As shown in Fig. 3d, through the arrangement of electric field lines, it can be found that the negative polarization charges at the tip of the nanocone are not only coupled with the positive polarization charges on the surface of the nanocone, but also coupled with the positive polarization charges on the upper surface of the nanoplate, so the resonance mode at 900 nm is the dipole resonance (l = 1) of the Au cone-on-plate nanostructure.

Thus, our study focuses on the short-wavelength extinction peak. By changing the refractive index from 1.33 to 1.39, the short-wavelength extinction peak is gradually red-shifted. As shown in Table 2, ηB is increased from 300 to 433 nm/RIU. FOM is improved from 1.5 to 6.19 RIU^{-1}, which is mainly attributed to the reduction of the FWHM from 222 to 70 nm. In a word, the Au nanocone-on-plate structure has greatly improved the RI sensitivity.

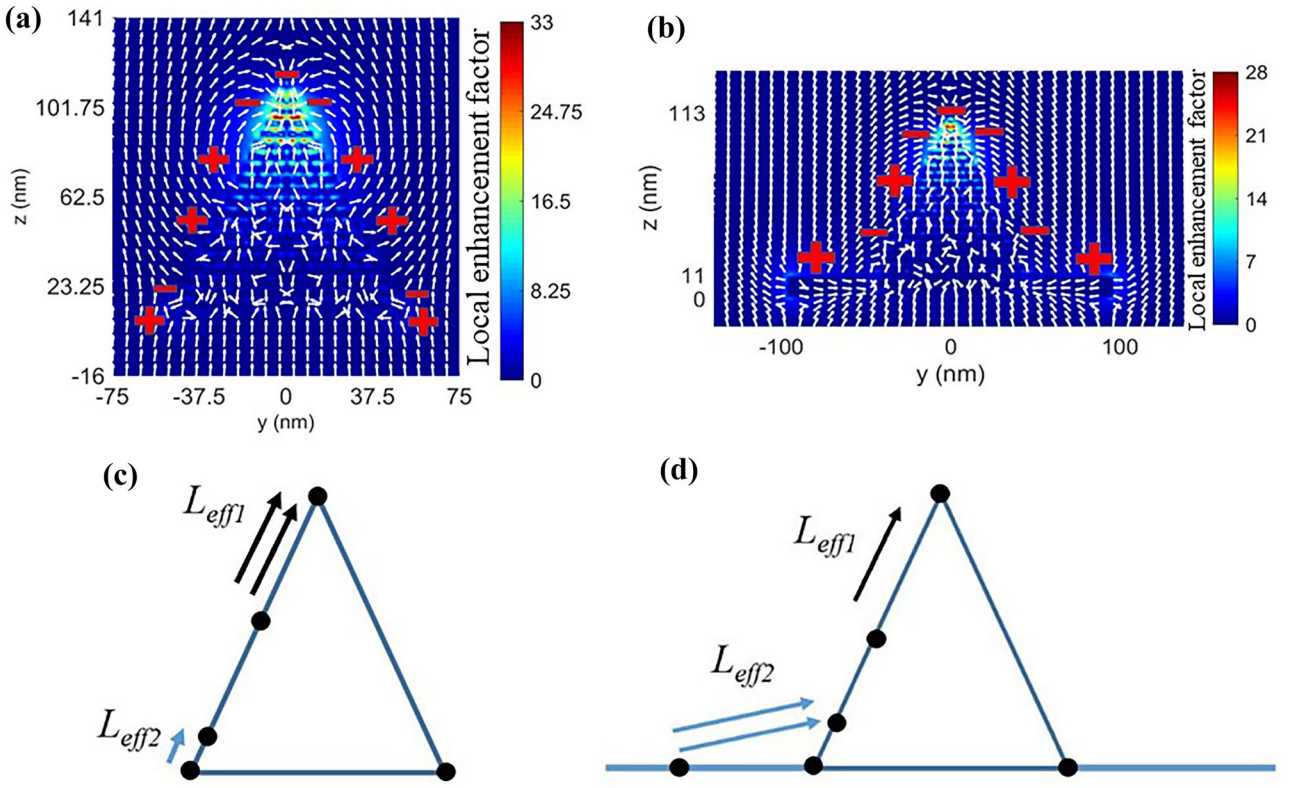

Fig. 5 The local electric field in the *yoz* plane of **a** Au nanocone. **b** Au cone-on-plate nanostructure. Two effective mean free paths of polarized charges corresponding to the multipole resonance (l = 3) of **c** Au nanocone. **d** Au cone-on-plate nanostructure

Multipole Plasmon Resonance in the Au Nanocone

In order to judge the resonance mode of the Au nanocone, it is necessary to analyze the cause of a small number of opposite charges distributed at the sides of the Au nanocone near the two endpoints. It is well known that the LSPR patterns of elongated nanostructures are more complex compared to the dipole resonance of symmetric nanoparticles, such as nanospheres [53]. Verellen et al. found that nanorods produce more resonance peaks with increasing aspect ratio. And the multipole resonance level of each peak is different. Similarly, the same pattern was found in the Au nanobipyramid. The multipole resonance (l = 3) is dominant in the Au nanobipyramid [35]. The Au nanocone has the characteristics of elongated nanostructures. To investigate the resonance mode of the Au nanocone, the extinction spectrum of the Au nanocone with D = 60 nm and *H* increasing from 50 to 100 nm has been calculated, as shown in Fig. 4a. It can be observed that with the increase of *H*, the Au nanocone exhibits more resonance peaks, which is in accordance with the principle of multipole resonance [54]. Taking the Au nanocone with *H* = 80 nm as an example, two obvious resonance peaks can be observed at 620 nm and 750 nm. By calculating the local electric fields at the two wavelengths along the *yoz* cross section through the center of the bottom surface and the tip, the polarized charges distributions are different, as shown in Fig. 4b, c. The local electric field at 620 nm produces a new positive polarized charge at the tip of the Au nanocone, which leads to an increase in the number of stages of multipole resonance. In order to prove that the charges of opposite polarity at the sides of the Au nanocone near the two endpoints are generated by the multipole resonance (l = 3) rather than by the coupling between the top surface of the Au nanoplate and the side of the Au nanocone, it is necessary to find the resonance wavelength corresponding to the dipole resonance (l = 1). According to the principle of multipole resonance, the resonance wavelength corresponding to the dipole resonance (l = 1) must be longer than the multipole resonance (l = 3), so we take any weak peak after 800 nm and simulate its local electric field, as shown in Fig. 4d. The upper half of the Au nanocone is distributed with positive polarized charges and the lower half of the Au nanocone is distributed with negative polarized charges, which is consistent with the distribution of dipole resonance. Therefore, it can be determined that the charges of opposite polarity on the side of the Au nanocone near the two end points are due to the multipole resonance. The resonance peak at 750 nm

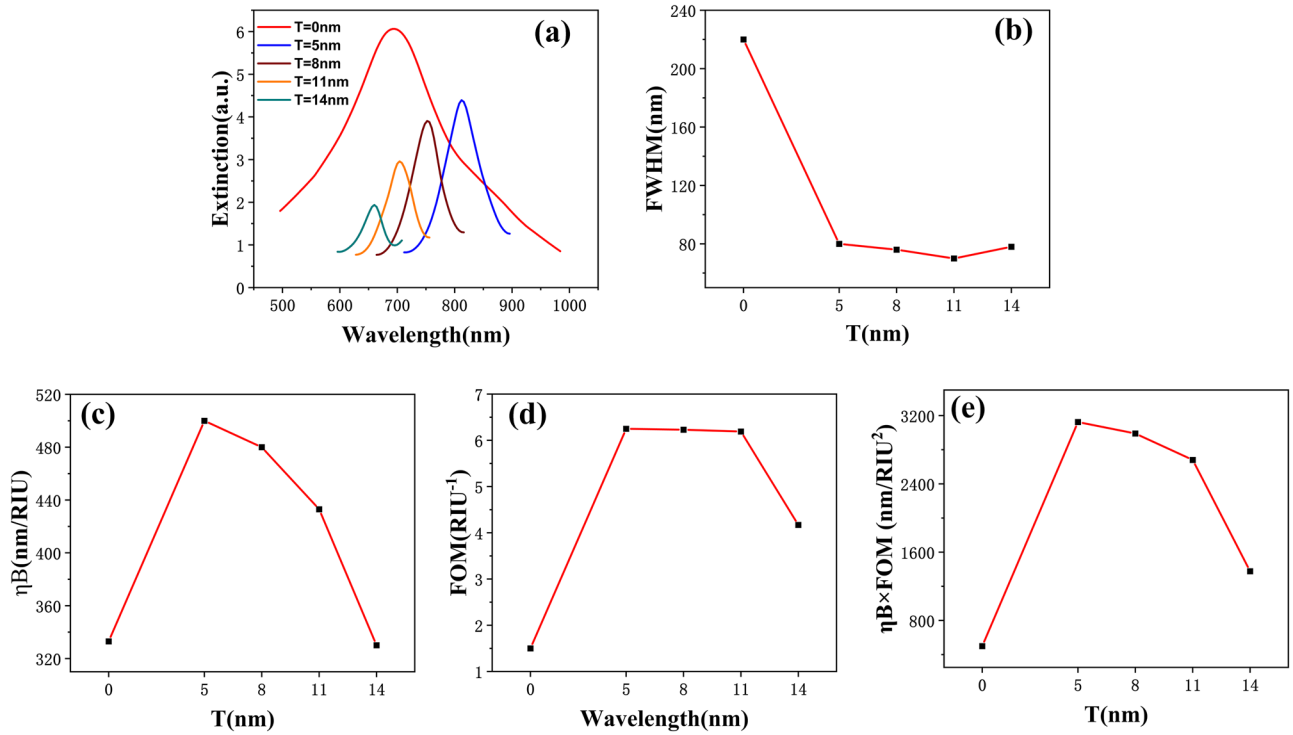

Fig. 6 **a** The extinction spectrum of the Au cone-on-plate nanostructure with $T=0$–14 nm, $n=1.33$. **b** FWHM with the change of T between 0 and 14 nm. **c** ηB with the change of T between 0 and 14 nm. **d** FOM with the change of T between 0 and 14 nm. **e** $\eta B \times$FOM with the change of T between 0 and 14 nm

corresponds to the multipole resonance (l=3) and the resonance peak at 620 nm corresponds to the multipole resonance (l=5).

According to the above results, the Au nanocone is dominated by the multipole resonance (l=3) and its dipole resonance is present, but the intensity is very weak. Therefore, the resonance peak at the short wavelength of the Au nanocone-on-plate nanostructure belongs to the multipole resonance (l=3).

Effective Mean Free Path of Polarized Charges in LSPR

It is well known that the damping of the LSPR is due to the scattering of electrons with phonons, electrons, lattice defects, or impurities. Proton resonance is a cooperative electron effect, implying that electron scattering leads to a loss of electron phase coherence, which in turn brings about an expansion of the proton absorption linewidth. Within the frame of the Mie theory, the FWHM of LSPR is given by [55]:

$$\Delta\Gamma = Av_F/L_{eff}$$

where $\Delta\Gamma$ is the linewidth of the LSPR band, v_F is the Fermi velocity [56], and L_{eff} is the effective mean free path of polarized charges [29]. A is the line-broadening constant, which is a dimensionless parameter, usually assumed to be close to unity, and is determined by details of the scattering process [30].

According to the above equation, L_{eff} is one of the most important factors affecting the FWHM. Through the local electric fields of the Au nanocone and the Au cone-on-plate nanostructure, we can draw the schematic diagram of the effective mean free path of polarized charges of both, as shown in Fig. 5. Since both belong to the multipole resonance (l=3), they all possess two pairs of polarized charges with opposite polarity. So L_{eff} consists of two effective mean free paths: L_{eff1} and L_{eff2}, which are respectively defined as the effective mean free path of the upper and lower pair of polarized charges with opposite polarity. From Fig. 5c, d, it is obvious to find that L_{eff2} in the Au cone-on-plate nanostructure is much larger than L_{eff2} in the Au nanocone, and the two L_{eff1} are not significantly different. According to the local electric field, L_{eff2} in the Au nanocone-on-plate structure has a larger proportion in L_{eff}, so the L_{eff} of the Au cone-on-plate nanostructure is larger than the L_{eff} of the Au nanocone, which causes the FWHM to be reduced from 200 to 70 nm.

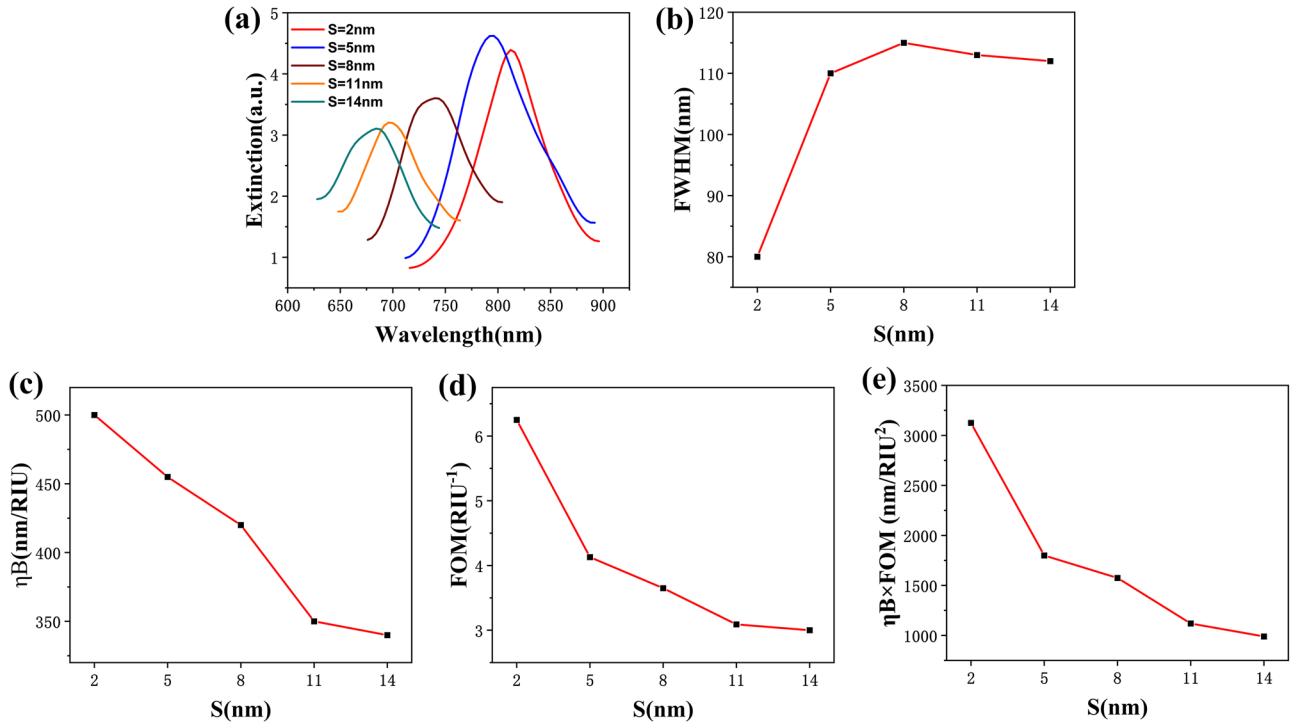

Fig. 7 **a** The extinction spectrum of the Au cone-on-plate nanostructure with $S=2$–14 nm, $n=1.33$. **b** FWHM with the change of S between 2 and 14 nm. **c** ηB with the change of S between 2 and 14 nm. **d** FOM with the change of S between 2 and 14 nm. **e** $\eta B \times$FOM with the change of S between 2 and 14 nm

The Effect of Thickness of the Au Nanoplate on RI Sensitivity

Due to the presence of the Au nanoplate, it can change the effective mean free path of polarized charges of multipole resonance (l = 3), thus substantially reduce the FWHM and improve the FOM. To investigate the effect of the Au nanoplate on the Au cone-on-plate nanostructure, the change of extinction spectrum by increasing T from 0 to 14 nm is shown in Fig. 6a. The FWHM with different T is counted in Fig. 6b. FWHM reaches the minimum value of 70 nm with $T=11$ nm. When the Au nanoplate is added, the extinction peak undergoes a certain red shift. However, the extinction peak is gradually blue-shifted with the increase of T. In order to investigate the effect of different T on the RI sensitivity, we change the refractive index from 1.33 to 1.39 and count its ηB, FOM, and $\eta B \times$FOM, as shown in Fig. 6c–e. It can be found that the Au cone-on-plate nanostructure with $T=5$ nm has the best sensing performance, with $\eta B=500$ nm/RIU, FOM = 7.25, and $\eta B \times \text{FOM} = 3125$ nm/RIU^2, and $\eta B \times$FOM is more than seven times that of the Au nanocone.

The Effect of Space Between the Au Nanoplate and the Au Nanocone on RI Sensitivity

By adjusting T in the previous section, the RI sensitivity of the Au cone-on-plate nanostructure is the best with $T=5$ nm, so T is set to 5 nm. We believe that the space between the Au nanoplate and the Au nanocone is also an important factor to influence the RI sensitivity. Therefore, by increasing S from 2 to 14 nm, the change in extinction spectrum is shown in Fig. 7a. Through the statistical results, it can be found that the FWHM shows a trend of increasing then decreasing with the increase of S. When $S=2$ nm, FWHM reaches the minimum value of 80 nm, as shown in Fig. 7b. In order to investigate the effect of S on the RI sensitivity, we change the refractive index from 1.33 to 1.39 and count its ηB, FOM, and $\eta B \times$FOM, as shown in Fig. 7c–e. It can be found that the three parameters decrease gradually with increasing S. When $S=2$ nm, $\eta B=500$ nm/RIU, FOM = 6.25, and $\eta B \times \text{FOM} = 3125$ nm/RIU^2. Therefore, the Au cone-on-plate nanostructure has the best sensing performance with $S=2$ nm.

By tuning T and S as described above, it was determined that the Au cone-on-plate nanostructure has the best RI

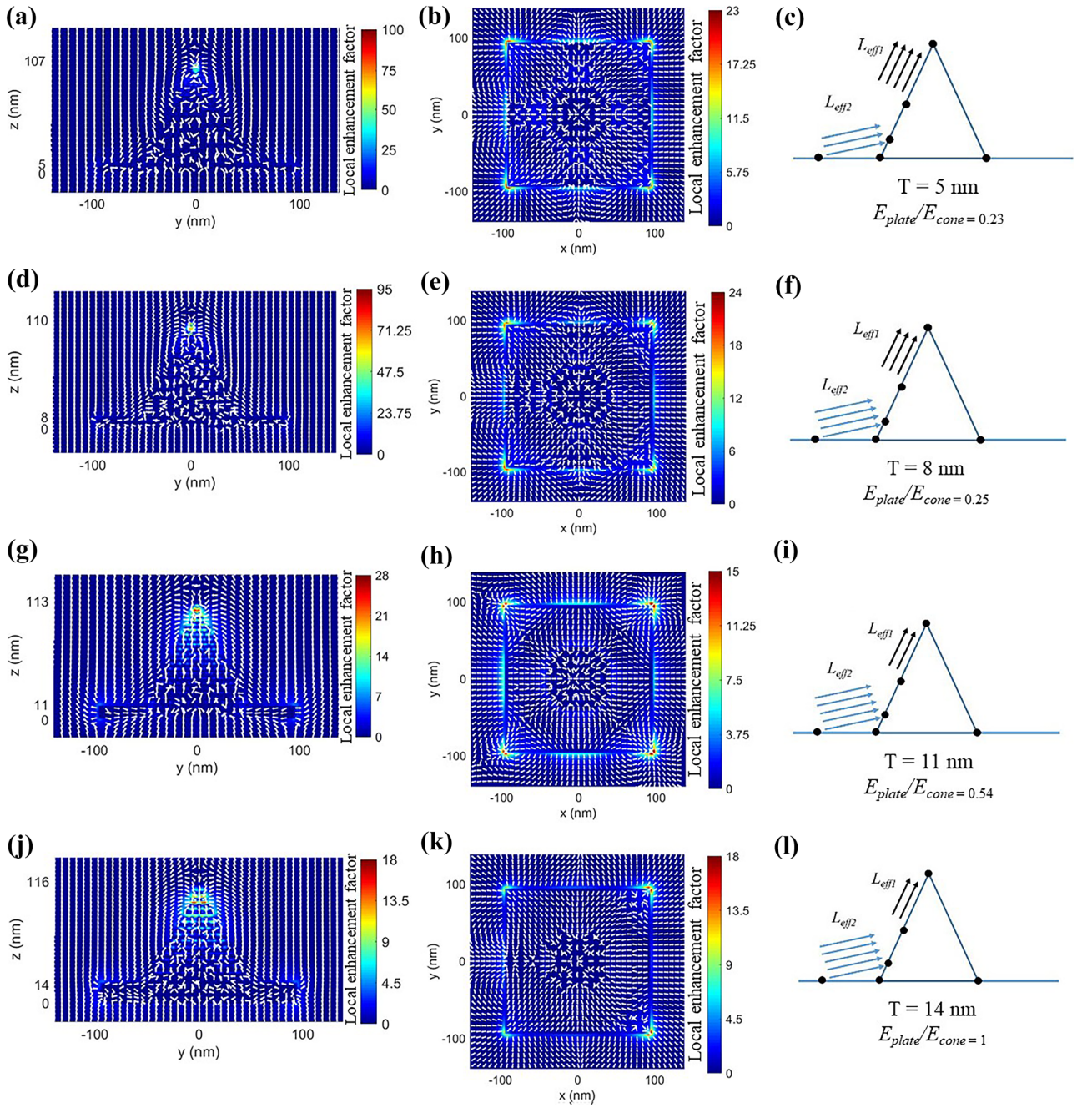

Fig. 8 The local electric fields in the *yoz* plane, *x*–*y* plane at the top surface of the Au nanoplate and the schematic diagrams of L_{eff1} and L_{eff2} of the multipole resonance (l = 3), **a**–**c** $T = 5$ nm, **d**–**f** $T = 8$ nm, **g**–**i** $T = 11$ nm, **j**–**l** $T = 14$ nm

sensitivity with $T = 5$ nm and $S = 2$ nm. Table 3 summarizes the comparison of the RI sensitivity between the Au cone-on-plate nanostructure and other previously reported Au plasmonic structures of other morphologies. The Au cone-on-plate nanostructure not only improves the sensitivity of the Au nanocone in all aspects, but also makes its RI sensitivity exceed that of other morphologies.

The Physical Mechanism of Altered RI Sensitivity by Au Cone-On-Plate Nanostructure

Our results show that T and S are important factors in changing the RI sensitivity. The local field explains that the Au nanoplate can affect L_{eff} to change the FWHM and thus the RI sensitivity. However, how do T and S specifically affect

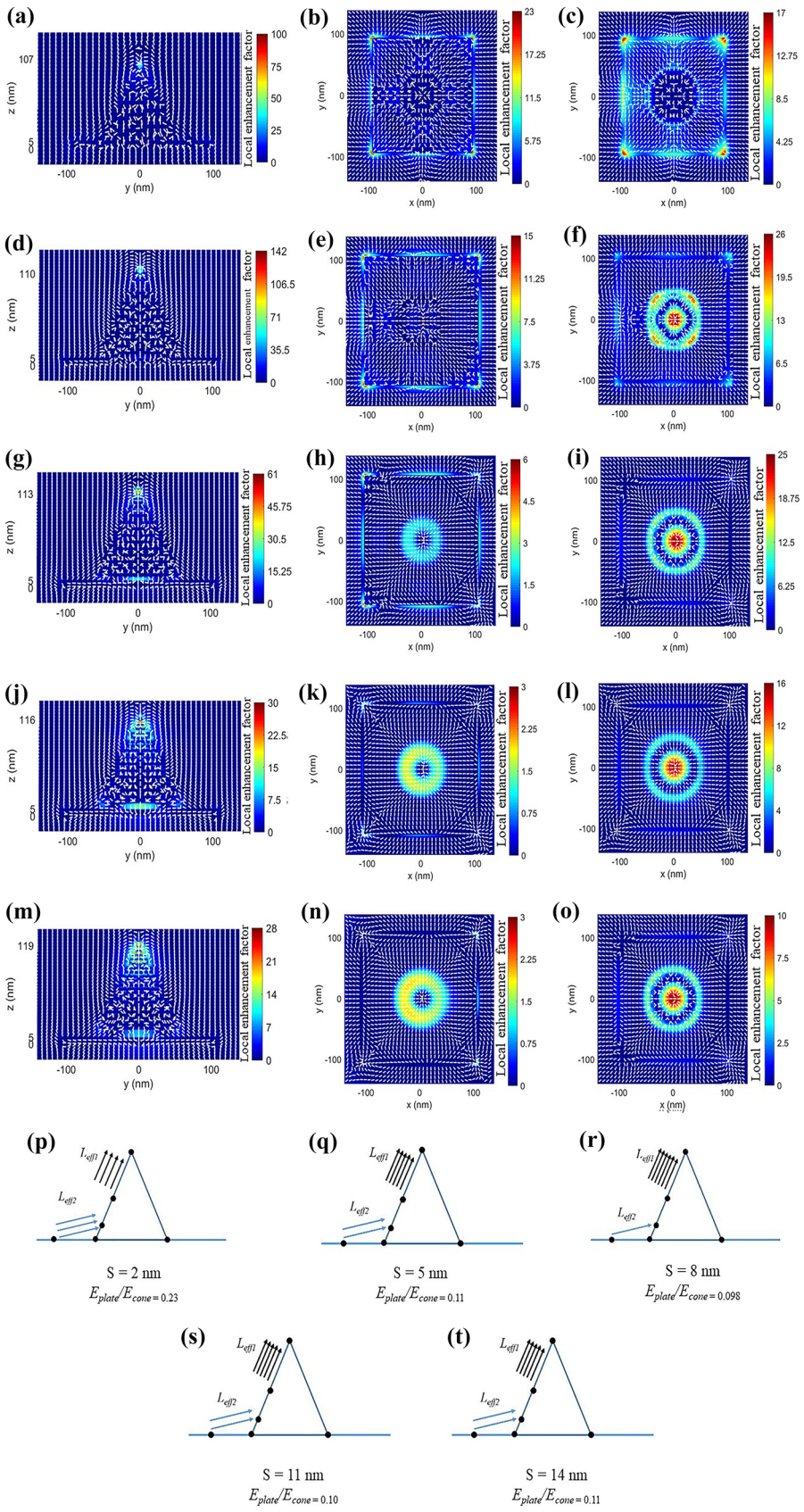

Fig. 9 The local electric fields in the *yoz* plane, *x*–*y* plane at the top surface of the Au nanoplate and *x*–*y* plane in the middle between the nanoplate and the nanocone of the multipole resonance (l = 3), **a**–**c** $S = 2$ nm, **d**–**f** $S = 5$ nm, **g**–**i** $S = 8$ nm, **j**–**l** $S = 11$ nm, and **m**–**o** $S = 14$ nm. **p**–**t** Schematic diagrams of $L_{eff}1$ and $L_{eff}2$ with different *S*

the polarized charge distribution? First, for the change of T, the local electric fields along the *yoz* cross section for different T, and the local electric fields of the x–y cross section on the top surface of the Au nanoplate are shown in Fig. 8. E_{cone} and E_{plate} are defined as the local field enhancement factor of the tip of the nanocone and the top surface of the Au nanoplate. The resonance of the Au nanoplate itself is very weak due to its small thickness. So E_{plate} is related to the lower pair of polarized charges with opposite polarity, and the upper pair of polarized charges with opposite polarity affects the E_{cone} in the multipole resonance (l = 3). The local field enhancement factor is proportional to the number of polarized charges [45]. So E_{plate}/E_{cone} can represent the proportion of L_{eff2} and L_{eff1} in the L_{eff}. It can be found that the higher the E_{plate}/E_{cone} is, the higher the proportion of L_{eff2} is, then the larger the L_{eff} is, and the smaller the FWHM is. According to Fig. 8, with the increasing of T from 5 to 11 nm, E_{plate}/E_{cone} increases from 0.23 to 0.54, so the FWHM is reduced from 80 to 70 nm, and the field enhancement factor of both parts has been weakened, so ηB is reduced. According to the calculation, FOM is reduced. But when T increases from 11 to 14 nm, the resonance of the Au nanoplate itself is enhanced, part of the polarized charges couple with the bottom surface of the nanoplate. Only the polarized charges which are close to the nanocone are involved in the multipole resonance (l = 3). The L_{eff2} decreases and is smaller than L_{eff1}, as shown in Fig. 8l. At the same time, the increase in E_{plate}/E_{cone} will cause the opposite effect on the L_{eff}. Therefore, the FWHM increases from 70 to 78 nm. Because the field enhancement factor continues to be weakened, the ηB continues to decrease and the FOM decreases. If T continues to increase, the resonance interference of the nanoplate itself will become stronger and the FWHM is gradually increasing, which has a negative impact on the RI sensitivity.

To explain the change of the RI sensitivity with different S, we calculate the local electric fields along the *yoz* cross section through the center and apex of the bottom surface corresponding to different S, the electric fields of the x–y cross section on the top surface of the Au nanoplate and the electric fields of the x–y cross section in the middle between the nanoplate and the nanocone. As shown in Fig. 9p–r, E_{plate}/E_{cone} decreases from 0.23 to 0.098 when S increases from 2 to 8 nm. This leads to FWHM increases from 80 to 115 nm. And we find that there is a significant increase and concentration of the field enhancement factor at the gap with the increase of S. This is mainly due to the suitable size of the gap, which has a strong electromagnetic attraction ability [60]. The interference at the gap leads to a decrease in the number of polarized charges involved in the L_{eff2}, resulting in a gradual decrease in E_{plate}/E_{cone}. When S continues to increase to 11 nm, E_{plate}/E_{cone} increases from 0.098 to 0.10, and then the FWHM decreases. Because the influence of the gap is gradually weakened. Continuing to increase S, the field enhancement factor of each part keeps almost unchanged. As the S increases, the hot spot intensity is also decreasing, so the ηB is decreasing.

Conclusion

In this paper, the RI sensitivity of the Au cone-on-plate nanostructure is investigated using the DDA method. The simulation results show that the main extinction peak of the Au nanocone corresponds to the l = 3 multipole resonance. Besides, we find that the Au cone-on-plate nanostructure can change the RI sensitivity by affecting the effective mean free path of polarized charges in multipole resonance (l = 3), which significantly influence the FWHM. The best sensing performance is achieved at $T = 5$ nm and $S = 2$ nm. The FWHM can be reduced from 220 to 80 nm, $\eta B = 500$ nm/RIU, FOM = 6.25 RIU^{-1}, and $\eta B \times FOM = 3125$ nm/RIU^2. This work offers new possibilities for improving RI sensitivity by changing the effective mean-free path of polarized charges. Moreover, the sensing capability of the Au nanocone is substantially improved, which makes it have better performance in practical detection.

Author Contribution Yu-Bo Guo: methodology; investigation; data curation; writing—original draft. Jian Zhu: conceptualization; formal analysis; writing—review and editing; supervision. Guo-Jun Weng: resources; supervision. Jian-Jun Li: conceptualization; resources; supervision. Jun-Wu Zhao: supervision.

Data Availability The data that support the findings of this study are available from the corresponding author upon reasonable request.

Code Availability Code data supporting the results of this study are available from the corresponding author upon reasonable request. The software used is DDSCAT.7.3

Declarations

Ethics Approval This is an observational study. The XYZ Research Ethics Committee has confirmed that no ethical approval is required.

Consent to Participate I would like to declare on behalf of my co-authors that the work described was original research that has not been published previously, and not under consideration for publication elsewhere, in whole or in part. All the authors listed have approved the manuscript that is enclosed.

Consent for Publication No conflict of interest exists in the submission of this manuscript, and the manuscript is approved by all authors for publication.

Conflict of Interest The authors declare no competing interests.

References

1. Zhu Q, Li P, Gao N, Hu X, Li C, Huang K, Kang J, Zhang R (2021) Deducing localized surface plasmon properties through analysis of the far-field optical spectra. J Phys D Appl Phys 55:015108
2. Wu D, Xu X, Liu X (2008) Electric field enhancement in bimetallic gold and silver nanoshells. Solid State Commun 148:163–167
3. Kozma E, Eckstein Andicsová A, Opálková Šišková A, Tullii G, Galeotti F (2022) Biomimetic design of functional plasmonic surfaces based on polydopamine. Appl Surf Sci 591:153135
4. Lindquist NC, Nagpal P, McPeak KM, Norris DJ, Oh SH (2012) Engineering metallic nanostructures for plasmonics and nanophotonics. Rep Prog Phys 75:036501
5. Chen Z, Chen H, Jile H, Xu D, Yi Z, Lei Y, Chen X, Zhou Z, Cai S, Li G (2021) Multi-band multi-tunable perfect plasmon absorber based on L-shaped and double-elliptical graphene stacks. Diam Relat Mater 115:108374
6. Zhang J, Xiao B, Zhao J, Li M, Lin H, Kang Z, Wu X, Liu H, Peng D-L, Zhang Q (2022) Understanding the growth mechanisms of metal-based core–shell nanostructures revealed by in situ liquid cell transmission electron microscopy. J Energy Chem 71:370–383
7. Zhang L, Jang HJ, Yoo S, Cho S, Won JH, Liu L, Park S (2018) Synthesis of octahedral gold tip-blobbed nanoparticles and their dielectric sensing properties. Nanotechnology 29:375602
8. Huang X, Zhang Z, Chen L, Lin Y, Zeng R, Xu J, Chen S, Zhang J, Cai H, Zhou H, Sun P (2022) Multifunctional Au nano-bridged nanogap probes as ICP-MS/SERS dual-signal tags and signal amplifiers for bacteria discriminating, quantitative detecting and photothermal bactericidal activity. Biosens Bioelectron 212:114414
9. Yang H, Zhao X, Zhang Z, Ma P, Wang X, Song D, Sun Y (2022) Biotin-streptavidin sandwich integrated PDA-ZnO@Au nanocomposite based SPR sensor for hIgG detection. Talanta 246:123496
10. Ruan X, Hulubei V, Wang Y, Shi Q, Cheng N, Wang L, Lyu Z, Davis WC, Smith JN, Lin Y, Du D (2022) Au@PtPd enhanced immunoassay with 3D printed smartphone device for quantification of diaminochlorotriazine (DACT), the major atrazine biomarker. Biosens Bioelectron 208:114190
11. Wen P, Yang F, Ge C, Li S, Xu Y, Chen L (2021) Self-assembled nano-Ag/Au@Au film composite SERS substrates show high uniformity and high enhancement factor for creatinine detection. Nanotechnology 32:395502
12. Yang Y, O'Riordan A, Lovera P (2022) Highly sensitive pesticide detection using electrochemically prepared Silver-Gum Arabic nanocluster SERS substrates. Sensor Actuat B: Chem 364:131851
13. Burris AJ, Cheng Q (2021) Plasmon-enhanced fluorescence in electrospun nanofibers of polydiacetylenes infused with silver nanoparticles. Langmuir 37:14920–14929
14. Kim J, Abbas N, Lee S, Yeom J, Asgar MA, Badshah MA, Lu X, Kim YK, Kim SM (2020) Fabrication of a Plasmonic nanoantenna array using metal deposition on polymer nanoimprinted nanodots for an enhanced fluorescence substrate. Polymers(basel) 13:48
15. Willets KA, Van Duyne RP (2007) Localized surface plasmon resonance spectroscopy and sensing. Annu Rev Phys Chem 58:267–297
16. Leitao C, Pereira SO, Alberto N, Lobry M, Loyez M, Costa FM, Pinto JL, Caucheteur C, Marques C (2020) Cortisol in-fiber ultrasensitive plasmonic immunosensing. IEEE Sens J 3028–3034
17. Mohiuddin AK, Jeon S (2022) Highly efficient Ag doped delta-MnO2 decorated graphene: comparison and application in electrochemical detection of H2O2. Appl Surf Sci 592:153162
18. Cai S, Gonzalez-Vila A, Zhang X, Guo T, Caucheteur C (2019) Palladium-coated plasmonic optical fiber gratings for hydrogen detection. Opt Lett 44:4483–4486
19. Zhang W, Liu T, Shan Y, Hou B, Chu Z, Gu X, Ma Z, Jin W (2021) In situ construction of oriented Pt-PANI needle-like nanoarrays-based label-free aptasensor for ultrafast and ultrasensitive recognition of cardiac troponin i. Adv Mater Interfaces 8:2101543
20. Zhu J, Zhang S, Weng GJ, Li JJ, Zhao JW (2021) Spiky yolk-shell AuAg bimetallic nanorods with uniform interior gap for the SERS detection of thiram residues in fruit juice. Spectrochim Acta A 262:120108
21. Wadhwa R, Ghosh A, Kumar D, Kumar P, Kumar M (2022) Platinum nanoparticle sensitized plasmonic-enhanced broad spectral photodetection in large area vertical-aligned MoS2flakes. Nanotechnology 33:255702
22. Ansah IB, Kim S, Yang JY, Mun C, Jung HS, Lee S, Kim DH, Kim SH, Park SG (2021) In situ electrodeposition of gold nanostructures in 3D ultra-thin hydrogel skins for direct molecular detection in complex mixtures with high sensitivity. Laser Photonics Rev 15:2100316
23. Reyes-Coronado A, Morales-Luna G, Vazquez-Estrada O, Garcia-Valenzuela A, Barrera RG (2018) Analytical modeling of optical reflectivity of random plasmonic nano-monolayers. Opt Express 26:12660–12683
24. Solis-Tinoco V, Morales-Luna G, Acevedo-Barrera A, Ochoa A, Vazquez-Estrada O, Olguin LF, García-Valenzuela A (2022) An optical sensor combining surface plasmon resonance, light extinction, and near-critical angle reflection, for thin liquid film biochemical sensing. Opt Laser Eng 158:107137
25. Sugawa K, Sugimoto D, Tahara H, Eguchi T, Katoh M, Uchida K, Jin S, Ube T, Ishiguro T, Otsuki J (2016) Refractive index susceptibility of palladium nanoplates with plasmonic resonance in the visible region. Opt Mater Express 6:859–867
26. Farooq S, Rativa D, de Araujo RE (2021) High performance gold dimeric nanorods for plasmonic molecular sensing. IEEE Sens J 21:13184–13191
27. Tam F, Moran C, Halas N (2004) Geometrical parameters controlling sensitivity of nanoshell plasmon resonances to changes in dielectric environment. J Phys Chem B 108:17290–17294
28. Takei H, Bessho N, Ishii A, Okamoto T, Beyer A, Vieker H, Golzhauser A (2014) Enhanced infrared LSPR sensitivity of cap-shaped gold nanoparticles coupled to a metallic film. Langmuir 30:2297–2305
29. Zhu J (2008) Local environment dependent linewidth of plasmon absorption in gold nanoshell: Effects of local field polarization. Appl Phys Lett 92:241919
30. Coronado EA, Schatz GC (2003) Surface plasmon broadening for arbitrary shape nanoparticles: a geometrical probability approach. J Chem Phys 119:3926–3934
31. Link S, El-Sayed MA (1999) Size and temperature dependence of the plasmon absorption of colloidal gold Nanoparticles. J Phys Chem B 103:4212–4217
32. Zhu J, Zhang F, Li J-J, Zhao J-W (2013) Optimization of the refractive index plasmonic sensing of gold nanorods by non-uniform silver coating. Sens Actuat B: Chem 183:556–564
33. Sun F, Yang W, Du C, Chen Y, Fu T, Shi D (2020) Optimal aspect ratio and excitation spectral region of LSPR sensors using individual Au dimmeric nanoplates. Plasmonics 15:949–955
34. Li Q, Zhuo X, Li S, Ruan Q, Xu Q-H, Wang J (2015) Production of monodisperse gold nanobipyramids with number percentages approaching 100% and evaluation of their plasmonic properties. Adv Opt Mater 3:801–812
35. Weng G, Shen X, Li J, Zhu J, Yang J, Zhao J (2021) Multipole plasmon resonance in gold nanobipyramid: effects of tip shape and size. Phys Lett A 412:127577
36. Cunha J, Guo TL, Koya AN, Toma A, Prato M, Della Valle G, Alabastri A, Proietti Zaccaria R (2020) Photoinduced temperature gradients in sub-wavelength plasmonic structures: the thermoplasmonics of nanocones. Adv Opt Mater 8:2000568

37. Zhu Q, Zhao X, Zhang X, Zhu A, Gao R, Zhang Y, Wang Y, Chen L (2020) Au nanocone array with 3D hotspots for biomarker chips. Cryst Eng Comm 22:5191–5199
38. Mi Y, Wen L, Xu R, Wang Z, Cao D, Fang Y, Lei Y (2016) Constructing a AZO/TiO2 core/shell nanocone array with uniformly dispersed Au NPs for enhancing photoelectrochemical water splitting. Adv Energy Mater 6:1501496
39. Fujiwara S, Kawasaki D, Sueyoshi K, Hisamoto H, Endo T (2022) Gold nanocone array with extensive electromagnetic fields for highly reproducible surface-enhanced Raman scattering measurements. Micromachines (Basel) 13:1182
40. Xu W, Bao H, Zhang H, Fu H, Zhao Q, Li Y, Cai W (2021) Ultrasensitive surface-enhanced Raman spectroscopy detection of gaseous sulfur-mustard simulant based on thin oxide-coated gold nanocone arrays. J Hazard Mater 420:126668
41. Ji P, Shi Q, Zheng L, Wang G, Chen F (2022) High sensitivity plasmonic refractive index and temperature sensor based on square ring shape resonator with nanorods defects. Opt Quant Electron 54:184
42. Wang Q, Zhu A, Qiu F, Wang L, Yin X-Y, Zhao W-M, Du N-N, Cong X-W, Ren Z-H, Hua L-R, Zhang K (2022) High sensitivity coreless fiber surface plasmon resonance sensor based on Au Nano biconical particles. IEEE Sens J 22:256–263
43. Shabaninezhad M, Kayani A, Ramakrishna G (2021) Theoretical investigation of optical properties of embedded plasmonic nanoparticles. Chem Phys 541:111044
44. Zhu J, Chen J-K, Li J-J, Zhao J-W (2019) Creating Orientation-independent built-in hot spots in gold nanoframe with multi-breakages. Plasmonics 14:1131–1143
45. Zhu J, Chen J-K, Li J-J, Zhao J-W (2019) Local dielectric environment-dependent plasmonic optical sensitivity of gold nanocage: from nanobox to nanoframe. Appl Phys A 125:62
46. Draine BT, Flatau PJ (2008) Discrete-dipole approximation for periodic targets: theory and tests. J Opt Soc Am A 25:2693–2703
47. Yurkin MA, Hoekstra AG (2011) The discrete-dipole-approximation code ADDA: capabilities and known limitations. J Quant Spectrosc Ra 112:2234–2247
48. Sosa IO, Noguez C, Barrera RG (2003) Optical properties of metal nanoparticles with arbitrary shapes. J Phys Chem B 107:6269–6275
49. Johnson PB, Christy RW (1972) Optical constants of the noble metals. Phys Rev B 6:4370–4379
50. Meng L-N, Zhu J, Weng G-J, Li J-J, Zhao J-W (2022) Optimization of the ultra-narrow plasmonic bandwidth of Pt-coated Au nanorod: the application in refractive index sensing. Physica E 135:114996
51. Morales-Luna G, Morales-Luna M (2021) Extinction coefficient modulation of MoO(3) films doped with plasmonic nanoparticles: from an effective medium theory description. Nanomaterials (Basel) 11:2050
52. Gerislioglu B, Dong L, Ahmadivand A, Hu H, Nordlander P, Halas NJ (2020) Monolithic metal dimer-on-film structure: new plasmonic properties introduced by the underlying metal. Nano Lett 20:2087–2093
53. Tabor C, Murali R, Mahmoud M, El-Sayed MA (2009) On the use of plasmonic nanoparticle pairs as a plasmon ruler: the dependence of the near-field dipole plasmon coupling on nanoparticle size and shape. J Phys Chem A 113:1946–1953
54. Verellen N, Lopez-Tejeira F, Paniagua-Dominguez R, Vercruysse D, Denkova D, Lagae L, Van Dorpe P, Moshchalkov VV, Sanchez-Gil JA (2014) Mode parity-controlled Fano- and Lorentz-like line shapes arising in plasmonic nanorods. Nano Lett 14:2322–2329
55. Garcia MA, De L, Crespo P, Llopis J, Penadés S, Fernández A, Hernando A (2005) Surface plasmon resonance of capped Au nanoparticles. Phys Rev B 72:241401–241404
56. Divliansky I, Mayer TS (2006) Three-dimensional low-index-contrast photonic crystals fabricated using a tunable beam splitter. Nanotechnology 17:1241–1244
57. Farooq S, Rativa D, de Araujo RE (2019) Optimizing the sensing performance of SiO2-Au nanoshells. Plasmonics 14:1519–1526
58. Miller MM, Lazarides AA (2006) Sensitivity of metal nanoparticle plasmon resonance band position to the dielectric environment as observed in scattering. J Opt A: Pure Appl Opt 8:S239–S249
59. Yang W, Chen Y, Fu T, Peng S, Du C, Lu Y, Shi D (2019) The cross-section shape-dependent responses of S and FOM of individual Au nanorod sensors. Appl Phys A 125:345
60. Zhu J, Zhao S-M (2015) A computational study of the giant local electric field enhancement in Al-Au-Ag trimetallic three-layered nanoshells. Plasmonics 11:659–667